PERGAMON

Building and Environment 36 (2001) 219–230

BUILDING AND ENVIRONMENT

www.elsevier.com/locate/buildenv

A preliminary investigation of airflow field in designated refuge floor

W.Z. Lu[a,*], S.M. Lo[a], Z. Fang[b], K.K. Yuen[a]

[a]*Department of Building & Construction, City University of Hong Kong, Kowloon, Hong Kong*
[b]*Department of Architecture and Civil Engineering, Wuhan University of Hydraulic and Electric Engineering, Wuhan, 430072, People's Republic of China*

Received 12 July 1999; received in revised form 27 September 1999; accepted 24 November 1999

Abstract

Refuge floor is specially designed in high-rise buildings for the purpose of supplying a temporarily safe place for evacuees under emergency situations. The provision of such designated refuge floor is a prescriptive requirement in the fire code of Hong Kong. Such a provision appears to be desirable by the regulators as it relates to simple rules and has administrative convenience. In order to fulfill its function, the refuge floor should be a safe place for the evacuees. The safeness of refuge floors under fire situations may be impaired if the floor is affected by smoke from lower levels. The code prescribes that cross-ventilation should be provided in refuge floor so as to prevent smoke logging. However, the adequacy of such a measure and the influence of such an open floor on the rest of building have not been analytically studied. An investigation on the airflow around and inside the refuge floor is required and will provide preliminary insight on the airflow and the smoke movement patterns. In this paper, the Computational Fluid Dynamics method is employed to analyze the airflow field around and inside a refuge floor. The aim of this paper is to describe the airflow field in and around a designated refuge floor, which is the first step to explore the wind effect on the safeness of refuge floors. The study shows that airflow could be a factor affecting the smoke flow pattern.

Keywords: Refuge floor; Numerical simulation; Cross ventilation; High-rise building

1. Introduction

The space available for erecting buildings in Hong Kong and many other metropolitan cities in Asia is limited. Growth of population, changes in family structure and expansion in business activities cause the demand for built space increasing rapidly in the past two decades. Numerous high-rise or ultra high-rise buildings[1] (e.g. office, commercial and residential buildings) have been erected in the recent decade and those are normally over 40 storeys. This implies that a large number of people in the Asian region live and work at a high level. There is no doubt that the government authorities, the building designers as well as the people of these cities are concerned for the design of high-rise buildings especially for the provisions related to the safety of the occupants inside these buildings. In relation to the emergency escape from high-rise buildings, the Hong Kong Government has stipulated in the Code of Practice on Means of Escape [1] that designated refuge floors should be provided in some of these buildings.

The provision of an area for refuge purpose is not a new concept. For example, in the NFPA101 Life Safety Code [2], the functions of refuge areas are expressed as to improve the usability of means of escape for the occupants of building, and to provide great flexibility in the provision of means of escape.

* Corresponding author.

[1] In this paper, high-rise buildings refer to those buildings over 30 m height in which firemen's lift is normally required, and ultra high-rise buildings refer to those buildings over 40 storeys.

0360-1323/00/$ - see front matter
PII: S0360-1323(00)00008-1

Nomenclature

B	width of the building
C_1 C_2 C_μ	Turbulent constants
C_p	pressure coefficient
H	height of the building
I_u	scaled turbulence intensity
k	kinetic energy of turbulence ($\frac{1}{2}$ $u_i u_i$)
L	length of the building (m)
p	pressure
P_k	turbulent generation term
U	velocity (m/s)
U_B	front edge velocity at roof (m/s)
u	velocity (m/s)
u_g	velocity at the height of z_g (m/s)
x	co-ordinates
z_g	the gradient height

Greek symbols

α	open exposure coefficient (0.15)
ε	turbulent energy dissipation rate (m^2/s^3)
δ_{ij}	the Kronecker symbol
κ	von Carmen constant, $\kappa = 0.4$–0.44
ν	kinematic viscosity (m^2/s)
ν_t	turbulent kinematic viscosity (m^2/s)
ρ	density (kg/m^3)
σ_k	Prandtl number of k
σ_ε	Prandtl number of ε

Subscripts

i	co-ordinate direction
j	co-ordinate direction
τ	transition point in boundary layer

However, the requirement to designate a complete floor for refuge purpose is apparently not included in the building or fire codes in most developed countries.

In the Hong Kong's code, a refuge floor is considered as a part of the exit route in a building, i.e. 'refuge floors should be provided in all buildings exceeding 25 storeys in height above the lowest ground storey, at not more than 20 storeys and 25 storeys respectively for industrial and non-industrial buildings from any other refuge floor'. Such refuge floor acts as a safe place for a short rest before people continue further escape actions as it is difficult for most people to walk down a tall building without pausing for more than 5 mins [3]. It also acts as a safe passage for people using one staircase once encountering smoke, fire or obstruction in that staircase, and enables them to proceed to an alternative staircase. Additionally, it acts as an assembly place for people to wait for rescue in case none of staircases can be used due to smoke, fire or obstruction. It is also argued that refuge floor may facilitate the evacuation process in high-rise buildings. It can serve as an image to release the stress of the evacuees and act as a staging point for firefighters and rescue people to initiate escape by using lifts [4].

Since the refuge floor is considered as a temporary safe place against fire, it should be protected from fire attack by components with sufficient fire resistance and adequate ventilation to prevent the retention of smoke [1]. As described in the code, every refuge floor should comply with the requirements: (a) there is no occupied accommodation or accessible mechanical plant room, except fire services water tanks and associated fire service installation plant room; (b) the net area for refuge should be not less than 50% of the total gross floor area of the refuge floor and should have a clear height of not less than 2.3 m; (c) the area for refuge should be open-sided above safe parapet height on at least two opposite sides to provide adequate cross ventilation; the open sides should comply with the requirements for fire resisting construction.

The code prescribes that cross ventilation should be provided in refuge floor so as to prevent smoke logging and guarantee the safeness of refuge floors. However, the safeness of refuge floors under fire situations may be impaired if the floor is affected by smoke dispersed from other levels. The smoke dispersion, under fire situation, may be affected by the position of fire source, the presence of wind (i.e. airflow pattern around building and inside refuge floor), and the configuration of buildings, etc. The knowledge on these aspects may have particular importance to the building designers. However, the studies in these areas are very limited. A preliminary study of wind effect on a high-rise building with a designated refuge floor will be presented and discussed in this paper.

Generally, a direct understanding of wind effect on buildings can be obtained from experimental studies in wind or salt-water tunnels. However, experimental studies are time-consuming and expensive. In addition, a scaled-model of designated refuge floor in a high-rise building within the atmospheric boundary is not easy to establish because the dimensional scale of refuge floor is relatively too small compared with the size of whole building (it is usually less than 3 m high in a building with height over 100 m). On the other hand, the wind flow around buildings is extremely complex as described by Hunt et al. [5]. The flow is always three-dimensional and involves severe pressure gradients, streamlined curvature, separation and reattachment, high turbulence levels and swirls, etc. [6]. When

considering other parameters such as transport phenomena of momentum, heat and smoke contaminant by convection, diffusion and radiative heat transfer, it will become more difficult to comprehend individual parameter by only one scaled-model test since those parameters interact strongly [7].

Accordingly, numerical simulations can be regarded as alternative methods for wind tunnel tests. Significant progress and some promising results have been produced in the numerical simulation of wind engineering [6–16] since 1970s. It is demonstrated by a large number of publications that numerical techniques can be successfully used in various aspects such as to predict the pressure distributions, wind velocities and dispersion of pollutants around and inside buildings.

In this study, a Computational Fluid Dynamics (CFD) technique is applied to analyze wind effect on a high-rise building with designated refuge floor and airflow field inside a refuge floor, which are expected to provide preliminary information for building design about how the existence of designated refuge floor in high-rise building influences the wind loading on building surfaces and the airflow pattern around building and inside the refuge floor. The numerical results will be validated by the available scaled-model test in wind tunnel [12]. The study can also be considered as the first step to explore the smoke effect on refuge floor.

2. The mathematical model

A full-scale three-dimensional CFD simulation is carried out to predict the air movement around and inside refuge floor and wind loading on the building surfaces. The geometrical configuration of the model is shown in Fig. 1. The airflow studied is considered as three-dimensional, steady, isothermal, incompressible and turbulent flow.

2.1. General governing equation

The fundamental equations governing the motion of steady, incompressible and turbulent flows are the averaged Navier-Stockes equations and continuity equation that can be expressed as:

$$\frac{\partial U_i}{\partial x_i} = 0$$

$$U_j \frac{\partial U_i}{\partial x_i} = -\frac{1}{\rho}\frac{\partial P}{\partial x_i} + \frac{\partial}{\partial x_j}\left[\upsilon\left(\frac{\partial U_i}{\partial x_j} + \frac{\partial U_j}{\partial x_i}\right) - \overline{u_i' u_j'}\right]. \quad (1)$$

The turbulent fluxes of momentum ($\overline{u_i' u_j'}$) are important terms that govern turbulent diffusion and need to be specified by certain turbulence model to fulfill the closure of equation set. A number of turbulence models are available ranging from simple algebraic models to second-moment closure models having been developed during the past decades. For the simplicity, the Reynolds-averaged Navier–Stokes (RANS) approach is adopted in this study. The standard k–ε model, which is regarded as still the most successful

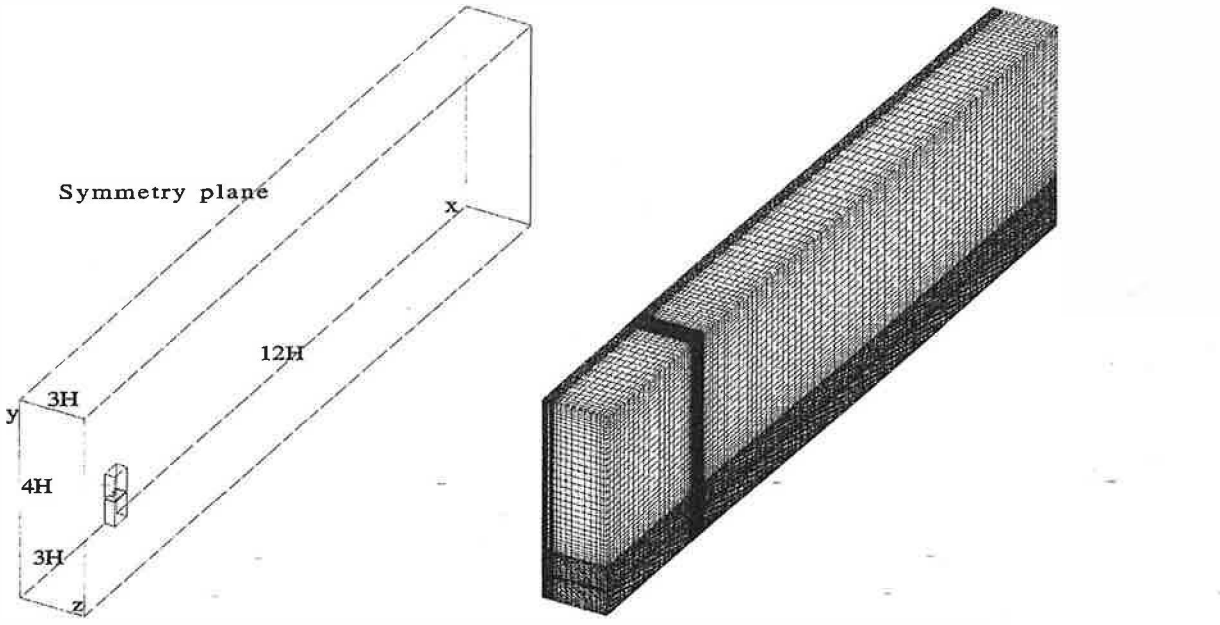

a. The flow domain b. The mesh scheme

Fig. 1. The geometrical configuration and mesh scheme. (a) The flow domain. (b) The mesh scheme.

turbulence model in engineering application at cost–effectiveness, is used for closing the equation set by virtue of the concept of turbulent viscosity. The k–ε model relates the turbulent diffusivity ν_t to the mean turbulent kinetic energy k and the dissipation rate of turbulence ε by:

$$\nu_t = C_\mu \frac{k^2}{\varepsilon} \quad \overline{u_i' u_j'} = -\nu_t \left(\frac{\partial U_i}{\partial x_j} + \frac{\partial U_j}{\partial x_i} \right) + \frac{2}{3} k \delta_{ij} \tag{2}$$

where δ_{ij} is the Kronecker symbol.

k and ε can be solved by the following transport equations:

$$U_j \frac{\partial k}{\partial x_j} = \frac{\partial}{\partial x_j} \left[\left(\nu + \frac{\nu_t}{\sigma_k} \right) \frac{\partial k}{\partial x_j} \right] + P_k - \varepsilon$$

$$U_j \frac{\partial \varepsilon}{\partial x_j} = \frac{\partial}{\partial x_j} \left[\left(\nu + \frac{\nu_t}{\sigma_\varepsilon} \right) \frac{\partial \varepsilon}{\partial x_j} \right] + C_1 P_k - \frac{\varepsilon}{k} - C_2 \frac{\varepsilon^2}{k} \tag{3}$$

$$P_k = \nu_t \frac{\partial U_i}{\partial x_j} \left(\frac{\partial U_i}{\partial x_j} + \frac{\partial U_j}{\partial x_i} \right).$$

The model constants are also to the standard values for wind-tunnel flows:

$c_\mu = 0.09$, $c_1 = 1.44$, $c_2 = 1.92$, $\sigma_\kappa = 1.0$ and $\sigma_\varepsilon = 1.3$.

The above equations are highly coupled, nonlinear types and are solved by iterations via the CFX code, based on a finite-volume method.

2.2. Physical description and grid creation

To simulate a general airflow pattern, a high-rise building, shown in Fig. 2(a), is considered. For comparison, the geometrical sizes of the building are 145 m high, 31 m wide and 31 m deep in accordance with the literature [12], in which, a corresponding scaled model (1:400) was measured in a wind tunnel test carried out by Stathopoulos et al. [8]. The refuge floor, with height of 2.5 m, is assigned in the middle of the building. The layout of the refuge floor is designated as direct-cross

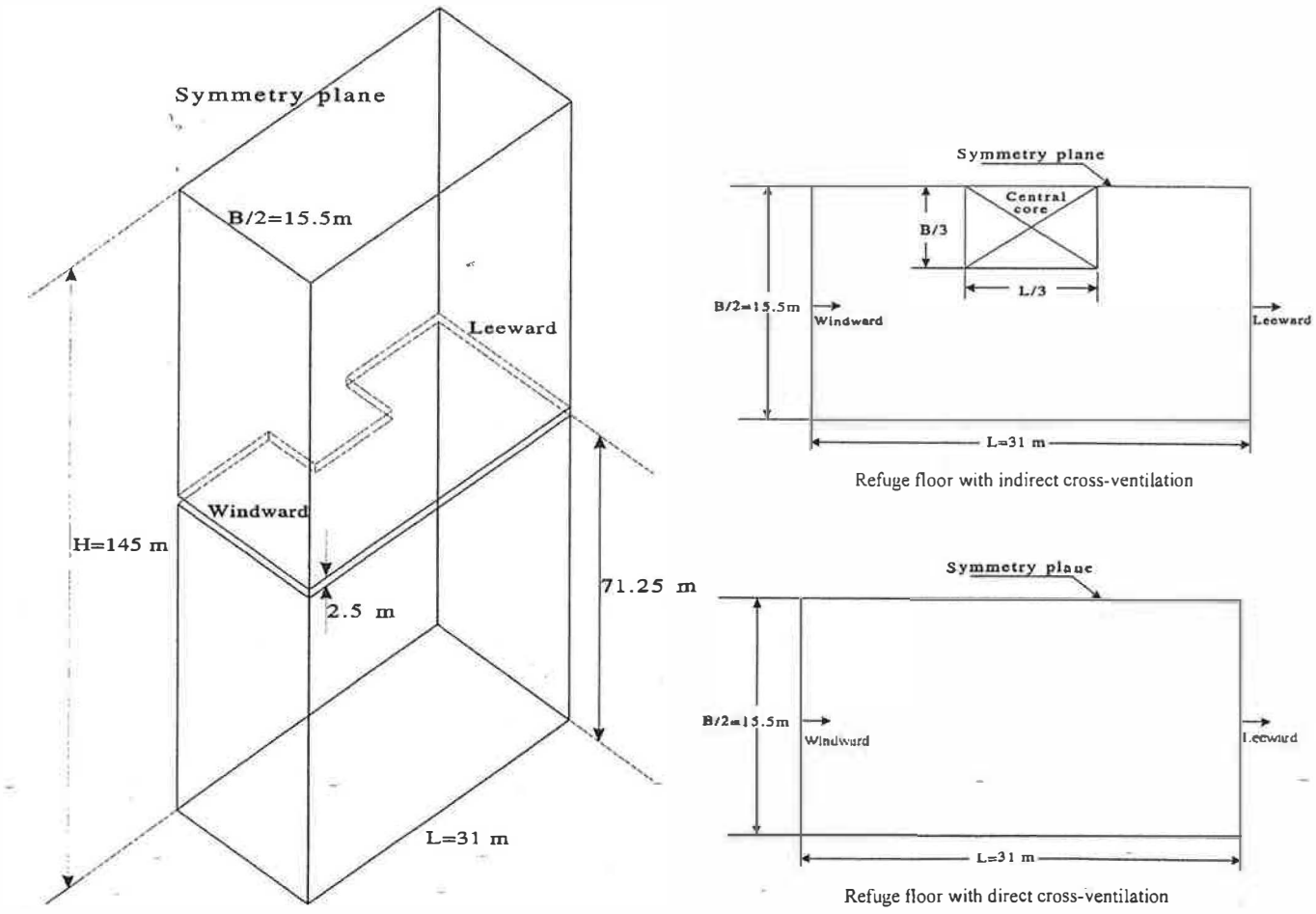

Fig. 2. The outlines of model building. (a) The building geometry. (b) The layout of refuge floor.

ventilation (without obstruction) and indirect-cross ventilation (with central core specified in the middle of the refuge floor), [see Fig. 2(b)].

As mentioned above, the dimensions of the refuge floor are relatively too small compared with the building sizes, fine meshes are required within the refuge floor and, in the mean time, for all areas close to wall surfaces. This causes difficulty to produce an appropriate computational mesh over the flow domain. To avoid the large aspect ratio in hybrid scheme discretization, which may cause numerical errors and convergence problem during the iterations, a mesh scheme of 23 × 6 × 11 grid nodes (length, height, width) is applied to the refuge floor. Considering the symmetry of flow pattern, only half of the physical domain along the symmetrical plane is taken into account to save the computational cost [see Fig. 1(a)]. The whole computational domain is divided into 119 × 79 × 24 control cells, which is shown in Fig. 1(b).

The scope of the computational domain should also be carefully handled. The narrow domain does not meet the Newman boundary condition that requires the fully developed boundary after the obstruction. To satisfy the Newman requirement, an upstream length of $x/H = 3$, a downstream length of $x/H = 12$, a height of $y/H = 4$ and a side width of $z/H = 3$ are assigned for the flow domain [see Fig. 1(a)].

2.3. Boundary conditions imposed on flow simulation

The inlet velocity conditions employ the power-law profile listed below:

$$\frac{u}{u_g} = \left(\frac{Z}{Z_g}\right)^{\alpha} \quad v = 0 \quad W = 0 \tag{4}$$

where α is called the open country exposure coefficient at the value of 0.15, Z_g is the gradient height, and u_g is the velocity at the height Z_g [12].

There is no standard method for setting k and ε but previous studies show that the inlet conditions specified for turbulence greatly influence the flow around bluff body, which is placed in atmospheric boundary layer [12]. For convenience, the turbulence intensity $I_u = \sqrt{u'^2}/U_o$ is established in accordance with the experimental conditions performed by Stathopoulos [8,12] expressed in Fig. 3. The turbulence energy and its dissipation rate are approximated using the following equations:

$$k(z) = 1.2 \cdot (I_u(z) \cdot U(z))^2 \tag{5}$$

$$\varepsilon(z) = \frac{C_\mu^{3/4} k(z)^{3/2}}{\kappa \cdot z}. \tag{6}$$

All solid boundary conditions, such as ground and building walls, are evaluated by the well-known wall function [15], in which the normal velocity is set to zero, the tangential velocity follows the logarithmic law $U(z) = U_\tau \ln(z/z_0)/\kappa$.

In simulation processes, the above highly coupled, nonlinear partial differential equations are firstly discretized into a set of linear algebraic equations, then solved by iteration solution on each control cell defined over the computational domain. A balance within source terms, convention and momentum fluxes is evaluated by continuity equation at the faces of each cell. All computations are proceeded by using CFX code, in which the above mathematical model has been installed.

3. Numerical analysis and discussion

3.1. Comparison between numerical simulation and measurement

The numerical results can be obtained by iterating the above discretized equations. The normalization of predicted pressure is based on the following formation:

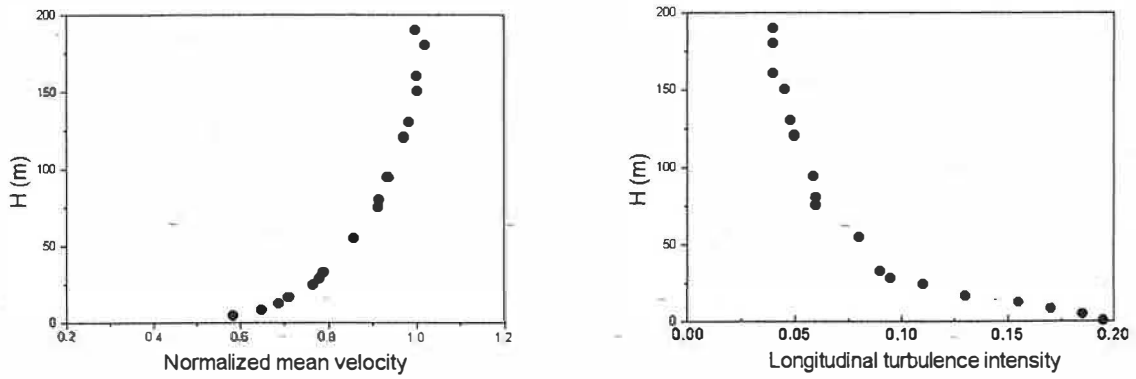

Fig. 3. Inlet velocity and turbulence intensity.

Mean pressure coefficient: $C_p = \frac{p - p_0}{\frac{1}{2}\rho U_B^2}$. (7)

Fig. 4 shows the comparisons of predicted and measured [12] pressure coefficient on the windward side and the roof of the building. A good agreement between the measured and the predicted $C_p$values on the windward side can be observed. The largest deviation less than 5% can be found at the maximum pressure point, i.e. the front stagnation point of the building. However, the discrepancies between the measured and predicted pressure coefficients along the roof are countable and not satisfied. The reasons causing such deviations may be incurred by less sufficient mesh scheme, the limitation of turbulence model currently used, etc. According to previous studies [5–14], the separation region on the roof for low-rise building is restricted in small region compared to the situation for high-rise one, the numerical results from the k–ε model for low-rise building case can still show good accordance with experiments. However, for tall buildings, such separation areas become much larger on the roof and the drawback of k–ε model in predicting the reverse flow pattern over that part will be revealed and, in the mean time, influence the accuracy of numerical simulation [9]. Advanced turbulence models will be needed to improve the quality of prediction. In addition to the effect of turbulence model, discrepancy may also be caused by other reasons such as the proper description of inlet boundary conditions, and the uncertainty of wind tunnel experiment [8]. The wind flow over the roof of a high-rise rectangular building is very complex since it involves high turbulence, severe pressure gradients, separation and possible reattachment. This also makes the numerical modeling and evaluation of wind-induced pressures on roof very difficult. Although the errors of the pressure on the roof exist, the predicted pressure coefficients are of sufficient accuracy for analyzing the flow around the refuge floor.

3.2. Airflow around the building with designated refuge floor

In accordance with Hong Kong's Code of Practice on Means of Escape [1], a designated refuge floor should be open-sided on, at least, two sides to provide adequate cross ventilation. A very limited literature can be traced in this area. A pioneer research is carried out and reported herein. In the study, the building considered is assigned to three conditions, i.e. (i) with a designated refuge floor and direct-cross ventilation; (ii) with a designated refuge floor and indirect-cross ventilation; and (iii) without a refuge floor. Same inlet boundary conditions are specified for all three cases. The numerical results are presented in Figs. 5–7. Fig. 5(a) compares the pressure distributions on windward surface of the building under the three conditions. The evident differences on three pressure curves can be noticed around the refuge floor. A sudden pressure variation exists due to the opening of refuge floor on the front edge of the building for both direct- and indirect-cross ventilation. The pressures on windward surface are recovered to the same level as the case without refuge floor in a short distance after passing the opening of refuge floor. Fig. 5(b) presents the pressure distributions on leeward surface of the building for all three conditions. Under direct-cross ventilation condition, the pressure coefficient first reduces smoothly, at the vicinity of refuge floor, varies sharply and decreases to the lowest point within a very short distance. This is mainly caused by vorticity changes in separation region due to the flow crossing the refuge floor. The maximum reducing range in reverse pressure gradient is over 50% comparing to the highest point. It also means that a strong flow sep-

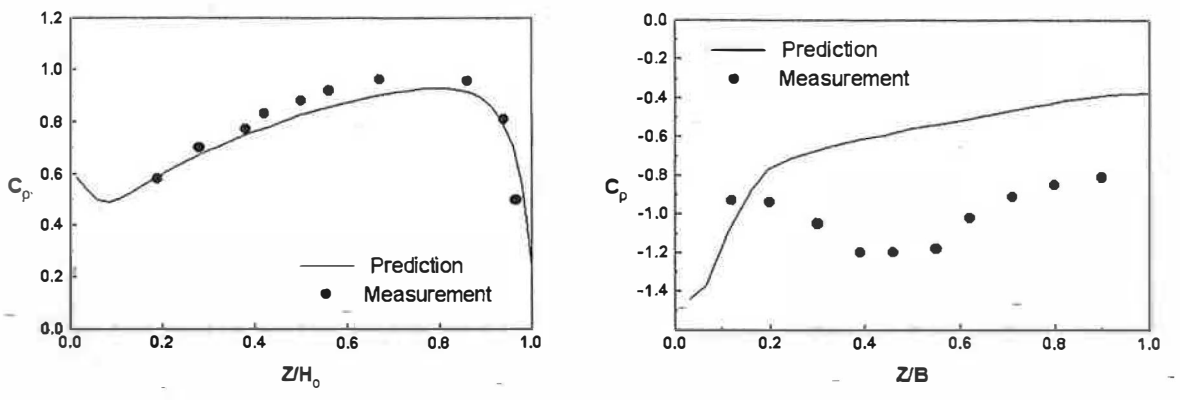

a. Pressure distribution on windward surface b. Pressure distribution on roof

Fig. 4. Comparison of pressure coefficients between predictions and measurements. (a) Pressure distribution on windward surface. (b) Pressure distribution on roof.

aration region occurs behind the refuge floor under direct-cross ventilation. The pressure gradually recovers, after the lowest point, to the normal level (i.e. the case without refuge floor). The results of indirect cross-ventilation show small differences from the case without refuge floor. Similar situations can be found on the roof surface in Fig. 5(c). There is almost no differences on pressure distributions along the roof between the case with indirect-cross ventilation and the case without refuge floor. Whilst the prediction of pressure under direct-cross ventilation is average higher than other two cases along the roof.

From Fig. 5, the differences in pressure distributions can be noticed between the two cross ventilation patterns at the vicinity of the refuge floor. The direct-cross ventilation produces lower pressure coefficient at the inlet of refuge floor of the building than the indirect-cross ventilation does. The higher resistance from indirect-cross ventilation obstructs the flow through the refuge floor partly, and causes a high reverse pressure gradient.

Fig. 6 shows the streamlines and velocity vectors around the building in the symmetry plane of flow domain with direct-cross ventilation. It seems that the airflow pattern does not have much difference between the conditions with and without refuge floor. The separation, reattachment, and streamline curvatures are similar to the pattern observed in wind-tunnel test by Stathopoulos et al. [12].

Comparisons of longitudinal velocity profiles between buildings with and without refuge floor along the main flow direction are shown in Fig. 7. The figure also demonstrates that the refuge floor does not significantly affect the whole flow field. From Fig. 7, almost no differences in velocity distributions can been observed between the situations with and without refuge floor except the area close to refuge floor. The location $x/B = 0.5$ represents the centerline of the building. A separation area exists behind the building. The zero velocity point on the downstream ground surface is identified as reattachment point. Corresponding to that point, the location $x/B = 6$ is close to the reattachment region. The value of x/H is approx. 2.5 H, i.e. the reattachment length. It agrees with most of wind-tunnel experimental results of wind flow around building [8], and also indicates that the stan-

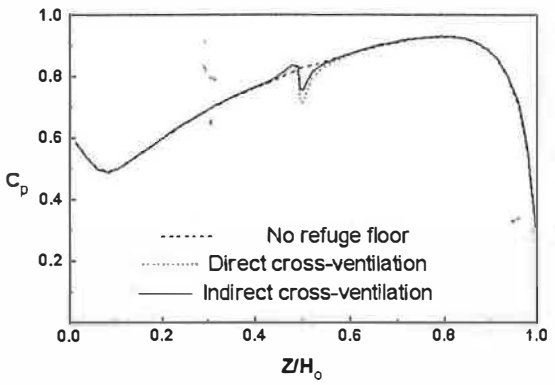

a. Pressure distribution on windward surface

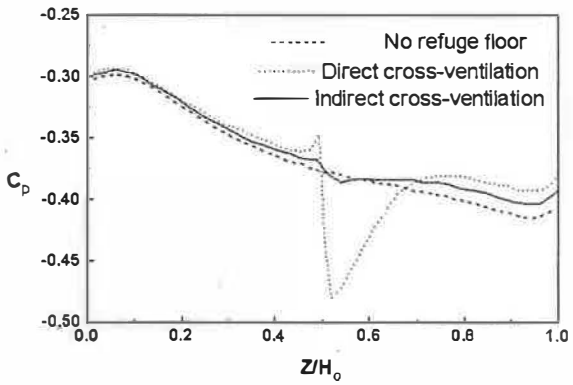

b. Pressure distribution on leeward surface

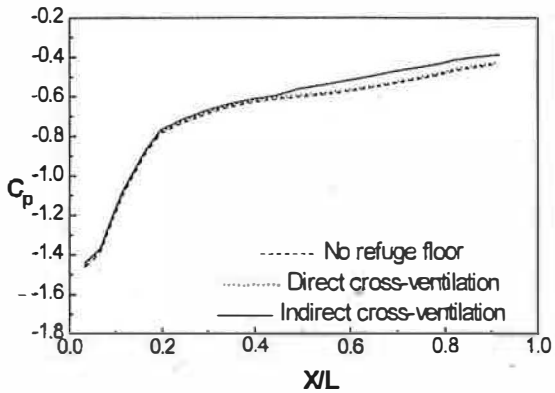

c. Pressure distribution on roof

Fig. 5. Pressure distributions on building surfaces. (a) Pressure distribution on windward surface. (b) Pressure distribution on leeward surface. (c) Pressure distribution on roof.

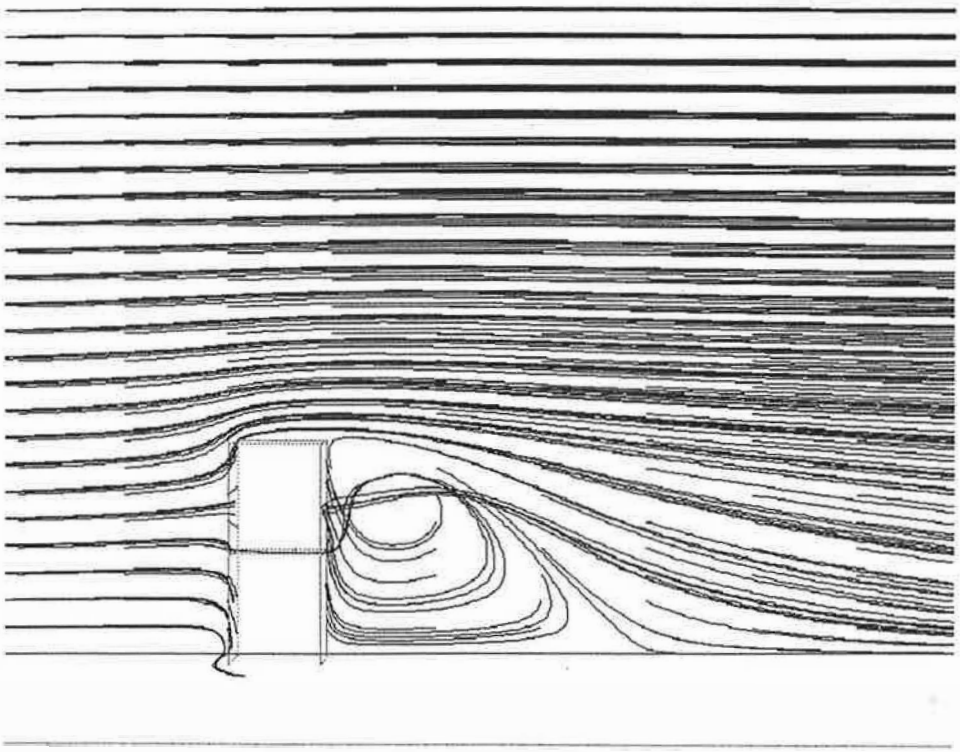

a. Streamlines around the building

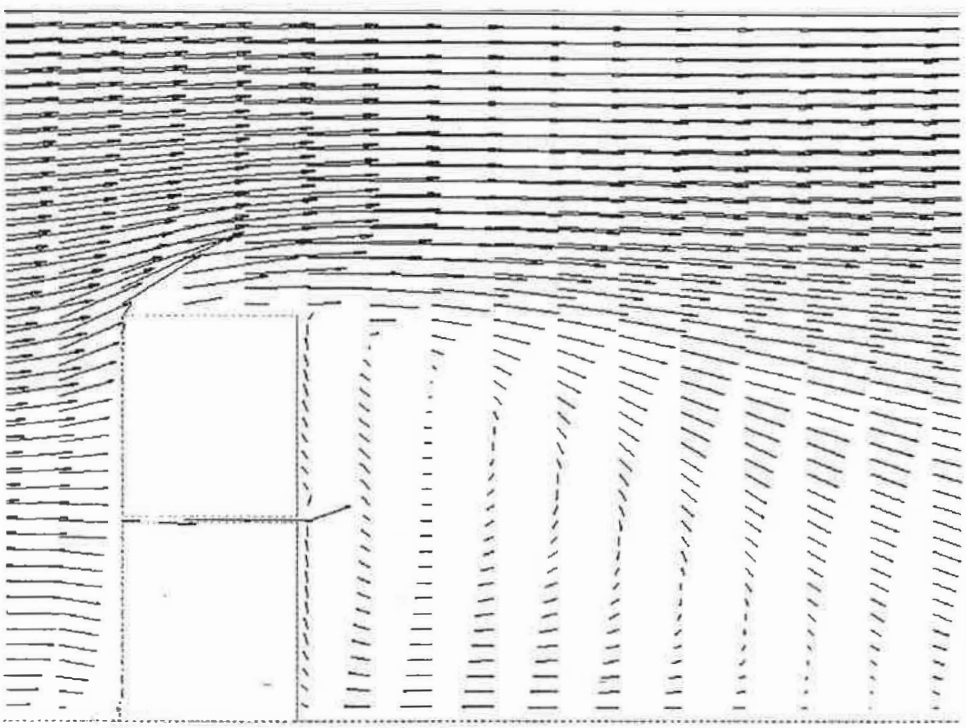

b. Airflow pattern around the building

Fig. 6. Airflow pattern around the building in symmetry plane. (a) Streamlines around the building. (c) Airflow pattern around the building.

dard k–ε model is suitable for analyzing the airflow field in the cases specified in this paper.

3.3. The air movement in the designated refuge floor

The airflow characters inside the refuge floor greatly influence the smoke diffusion, dilution and elimination in case smoke spreads into the refuge floor. Fig. 8 represents the airflow patterns passing the refuge floor with both direct- and indirect-cross ventilation. The flow pattern around the internal core in the indirect-cross ventilation case is in accordance with the characteristic of flow around a bluff body. A symmetrical pair of vortexes exists behind the core in the floor [Fig. 8(a)]. In Fig. 8(b), the airflow directly cross the refuge floor without obstruction, and a greater velocity in the floor can be noticed.

Fig. 9 expresses the velocity distributions at the inlet and outlet along the height of the refuge floor under two ventilation conditions (i.e. direct- and indirect-

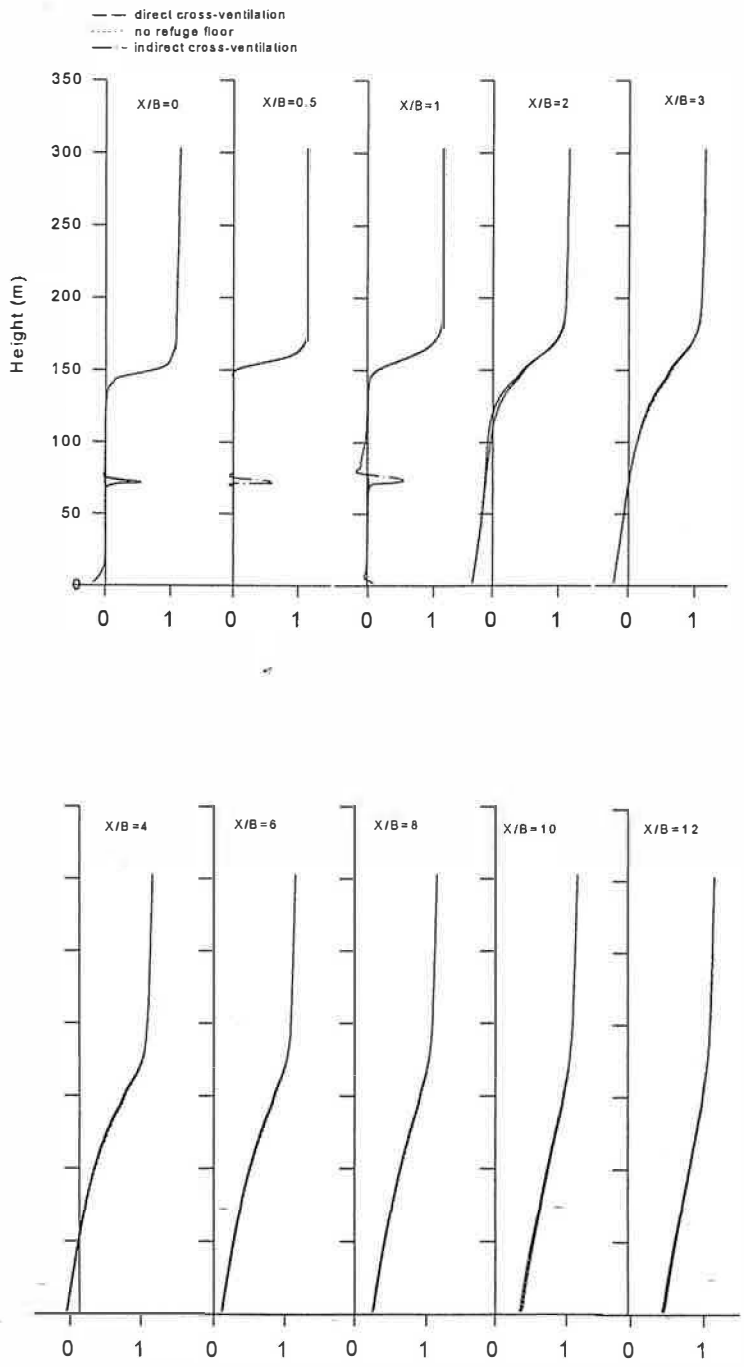

Fig. 7. Longitudinal velocity in symmetry plane of the building with refuge floor along the main flow direction.

cross ventilation). The differences between the two kinds of cross ventilation conditions can be seen in the vertical plane of the refuge floor. Generally, the velocities in direct-cross ventilation case are greater than that in indirect-cross ventilation condition. Furthermore, velocity distributions are found to skew to the lower levels of the floor under both ventilation conditions. Such phenomenon may be caused due to separation induced and the obstruction of the lower front corner of the refuge floor. Although part of airflow has been released suddenly over the refuge level after the front corner, it is still squeezed by the front surface

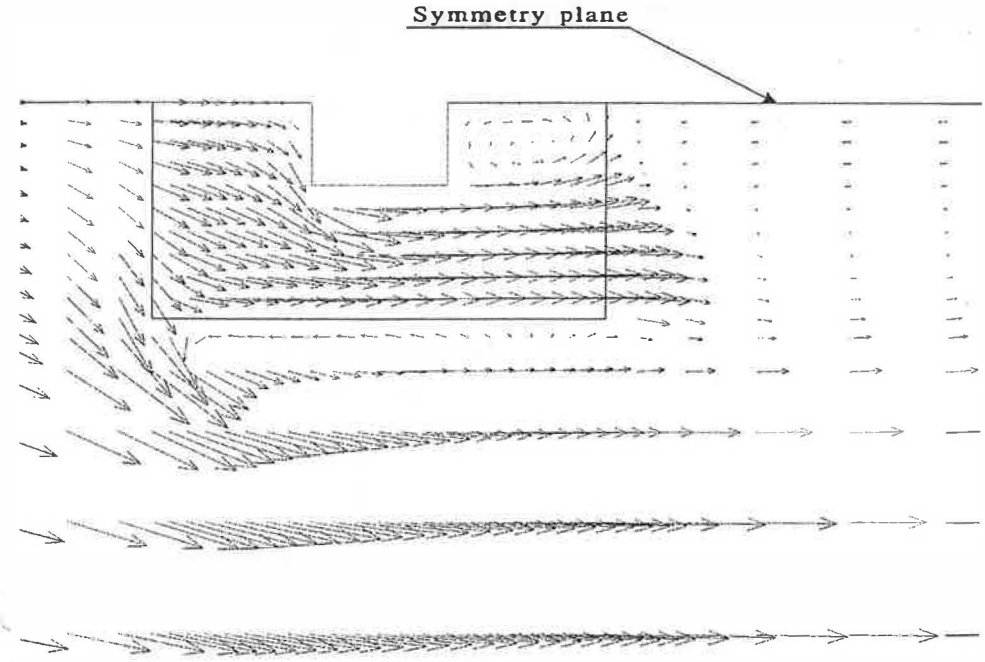

a. Air movement in refuge floor with indirect cross-ventilation

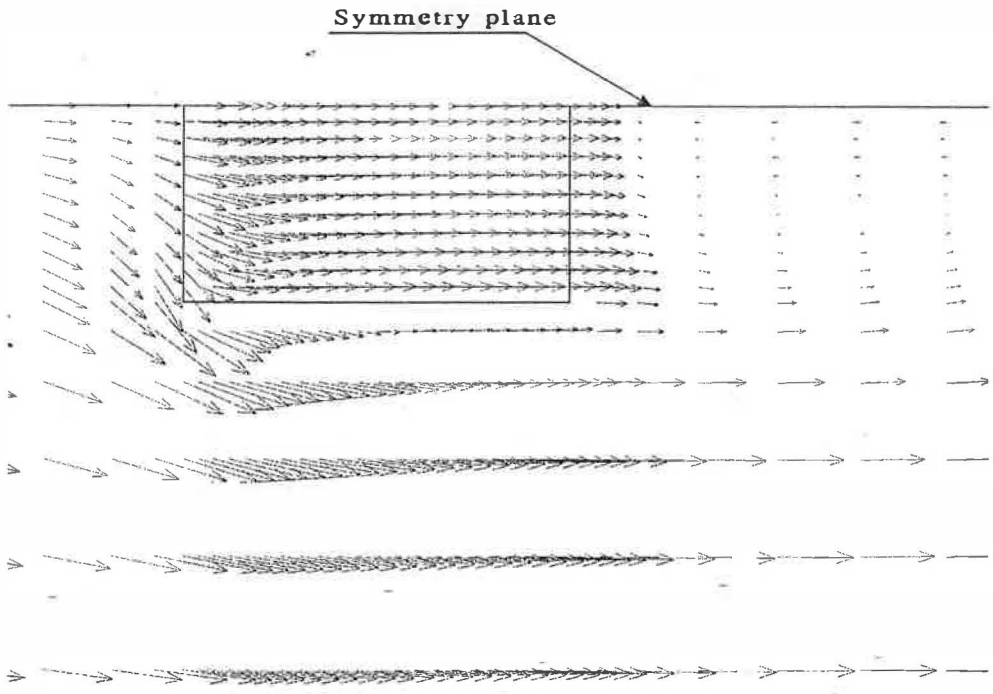

b. Air movement in refuge floor with direct cross-ventilation

Fig. 8. Airflow pattern within refuge floors. (a) Air movement in refuge floor with indirect-cross ventilation. (b) Air movement in refuge floor with direct-cross ventilation.

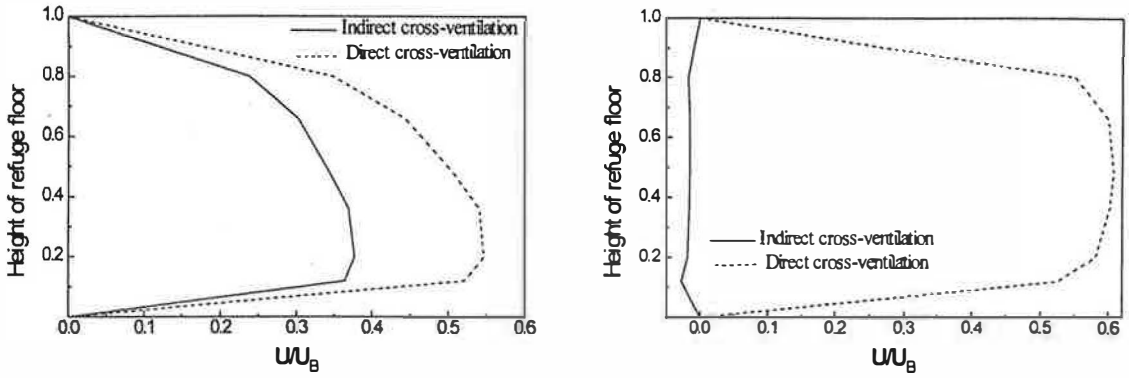

Fig. 9. The velocity distributions along the height of the refuge floor. (a) Velocity profile at inlet. (b) Velocity profile at outlet.

of building under the refuge floor. It attributes to similar mechanism as flow passing the front roof corner of the building.

Fig. 10 indicates the velocity profiles in horizontal plane along the width of the refuge floor. It appears that the flow pattern at the windward side of the refuge floor is close to parabolic. The low velocity region concentrates to side-wall surface. The direct-cross ventilation produces higher speed at the windward side than the indirect one does. The velocity deficit occurs at the leeward sides for both cross ventilation situations. Such flow patterns contribute to the wake flow behind the building. In addition, a strong reverse velocity is found in the centerline plane under indirect-cross ventilation. The main reason is that the internal core within the refuge floor enhances the flow effect around blunt body, and produces a pair of vortexes behind it under indirect-cross ventilation.

From the above analyses, it can be seen that geometrical configurations in refuge floor do affect the velocity distributions and further the smoke diffusion in refuge floor. The results imply that high speeds will be produced in refuge floor under direct-cross ventilation, and may spread smoke quicker than that under indirect-cross ventilation once the smoke entering the refuge floor. The smoke, in anyway, is expected to be extracted or diluted as quickly as possible but, under indirect-cross ventilation, may be trapped and circulated inside the refuge floor due to the obstruction of central core, which is a typical design in high-rise buildings but not favorable to refuge floor. The study presented here can provide useful information to building designers on considering the planing of refuge floors within high-rise buildings.

4. Conclusions

A detailed numerical analysis of airflow around and within the designated refuge floor of a high-rise building has been presented in the paper. Following conclusions can be drawn:

1. Generally, the numerical results of wind loading on building surfaces express good and satisfactory agreements with the corresponding experimental data;
2. The presence of designated refuge floor have little

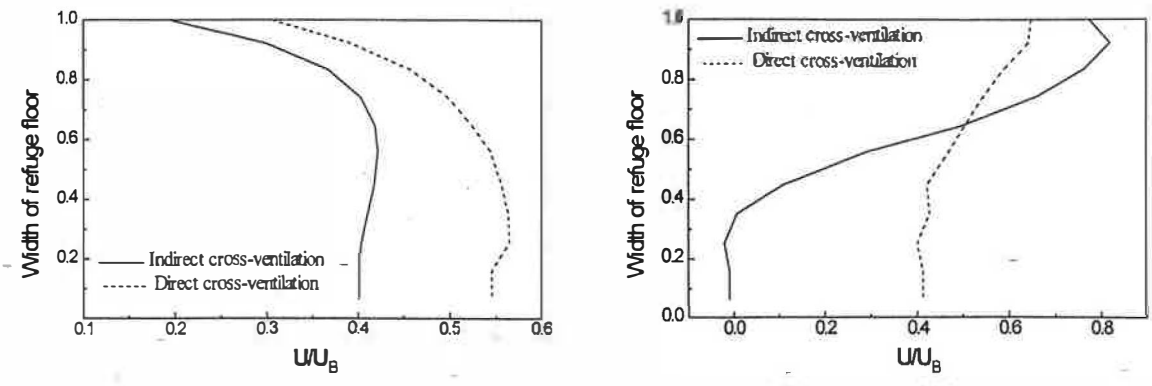

Fig. 10. The velocity distributions along the width of refuge floor. (a) Velocity profile at inlet. (b) Velocity profile at outlet.

influence on the airflow field around the building, so the total building responses to external environmental impact will not be affected;
3. The airflow pattern within the refuge floor is greatly influenced by the geometrical characteristics of the floor, and will further affect the smoke diffusion inside the refuge floor;
4. The refuge floor with direct-cross ventilation may assist to extract the smoke once it entering the floor, while the indirect-cross ventilation case may retards the smoke expelling due to the geometrical blockage (such design with central core is typical in high-rise buildings);
5. Further studies are required to help understand the smoke migration within the refuge floor and the effect of external airflow conditions on the smoke diffusions.

Acknowledgements

The authors acknowledge the support of the Strategic Research Grant #7000794, City University of Hong Kong.

References

[1] Code of Practice on Means of Escape, Hong Kong, Hong Kong Government, 1996.
[2] NFPA101, *Life safety code*. Quincy, MA: National Fire Protection Association, 1994.
[3] Egan MD. Concepts in building fire safety. Malabar, Fla: R. Krieger Publishing Co., 1986.
[4] Lo SM. The use of designated refuge floors in high-rise buildings: Hong Kong perspective. Journal of Applied Fire Science 1998;7(3):287–99.
[5] Hunt JRC, Abell CJ, Peterka JA. Kinematical studies of the around free or surface-mounted obstacles-applying topology to flow-visualization. Journal of Fluid Mechanics 1978;86:179–200.
[6] Paterson DA, Colin JA. Simulation of flow past a cube in turbulent boundary layer. Journal of Wind Engineering & Industrial Aerodynamics 1990;35:149–76.
[7] Murakami S, Ooka R. CFD analysis of wind climate from human scale to urban scale. In: International Workshop on "CFD for wind climate in cities", Hayama, Japan, 1998, 1998.
[8] Stathopoulos T. Computational wind engineering: Past achievements and future challenges. Journal of Wind Engineering & Industrial Aerodynamics 1997;67 & 68:509–32.
[9] Murakami S. Overview of turbulence models applied in CWE-1997. Journal of Wind Engineering & Industrial Aerodynamics 1998;74(76):1–24.
[10] Kim SE, Boysan F. Application of CFD to environmental flow. In: International Workshop on "CFD for wind climate in cities", Hayama, Japan, 1998, 1998.
[11] Ferziger JH. Approaches to turbulent flow computation: application to flow over obstacles. Journal of Wind Engineering & Industrial Aerodynamics 1990;35:1–19.
[12] Stathopoulos T, Brulotte MD. Design recommendations for wind loading on buildings of intermediate height. Canadian Journal of Civil Engineering 1989;16:910–916D.
[13] Paterson A, Apelt CJ. Computation of wind flow over buildings. Journal of Wind Engineering & Industrial Aerodynamics 1986;24:193–213.
[14] Paterson A, Apelt CJ. Simulation of wind flow around three-dimensional buildings. Journal of Building & Environment 1989;24:39–50.
[15] Launder BE, Spalding DB. The numerical computation of turbulent flows. Computer Methods in Applied Mechanics and Engineering 1974;3:269–89.